J. Wind Eng. Ind. Aerodyn. 126 (2014) 11–23

Contents lists available at ScienceDirect

Journal of Wind Engineering and Industrial Aerodynamics

journal homepage: www.elsevier.com/locate/jweia

A comparison of methods to estimate peak wind loads on buildings

Xinlai Peng [a], Luping Yang [a], Eri Gavanski [b], Kurtis Gurley [a,*], David Prevatt [a]

[a] University of Florida, Gainesville, FL, USA
[b] Tohoku University, Sendai, Japan

ARTICLE INFO

Article history:
Received 29 July 2013
Received in revised form
22 December 2013
Accepted 27 December 2013
Available online 28 January 2014

Keywords:
Peak pressure coefficient estimation
Gumbel distribution
Translation process
Low-rise building
Non-Gaussian process
Wind pressure
Comparative study
Wind tunnel

ABSTRACT

The most appropriate statistical technique to estimate a peak pressure coefficient from wind tunnel data is not a settled issue. The lack of a standard acceptable method can lead to inconsistent definitions and interpretations of peak pressure coefficients, particularly since time constraints associated with wind tunnel tests necessitate relatively short test durations. A Gumbel model is commonly used to represent the peak distribution, where parameters are determined using observed peaks. Recent papers have proposed several variations of a peak estimation procedure using the entire time history and a translation from a Gaussian peak distribution model to non-Gaussian. It is shown that, in the case of mildly non-Gaussian data, translation methods achieve accuracy comparable to the Gumbel method. It is also shown that translation methods lose accuracy when the record deviates significantly from Gaussian, while the Gumbel model maintains stable accuracy and precision. This paper presents two new translation-based peak pressure coefficient estimation schemes that offer accurate and stable performance for strongly non-Gaussian data. Very long duration wind tunnel data provide empirical peak distributions with which to compare the relative performance of the Gumbel, existing translation and proposed new translation methods. One of the new methods slightly outperforms the Gumbel method.
© 2014 Elsevier Ltd. All rights reserved.

1. Introduction

An important outcome from wind tunnel testing of low-rise buildings is a statistical assessment of peak pressure coefficients (C_{p_peak}), typically defined as a chosen fractile from a peak probability model whose parameters are determined from the observed data. The accuracy and precision (uncertainty) of this approach depend upon the form of the chosen peak probability model, the method used to identify its parameters, and the quantity of data available. In order to obtain an adequate tap resolution, large model scales are desirable for low-rise buildings. This leads to a decreased time scale and long data records to achieve the desired full-scale equivalent time. Thus, there is a trade-off between the uncertainty of the estimated C_{p_peak} and the desire to minimize data record lengths to limit the time and cost of wind tunnel experiments.

Many techniques for estimating C_{p_peak} have been proposed in the literature (Davenport, 1964; Gioffrè et al., 2000; Huang et al., 2013; ISO, 2009; Kwon and Kareem, 2011; Lieblein, 1974; Peterka, 1983; Sadek and Simiu, 2002; Stathopoulos, 1983; Tieleman et al., 2006). Each of them has unique advantages and disadvantages. This study concerns those methods that fall into one of two approaches: (1) determining C_{p_peak} from observed peaks (observed peak methods); and (2) mapping the peak distribution of a Gaussian process to a non-Gaussian peak cumulative distribution function (CDF) via the translation process (translation methods).

Observed peak methods include: a single observed peak value recorded during a sampling period (Stathopoulos, 1979), the mean of several observed maxima (Holmes et al., 1989), and a value corresponding to a chosen fractile from a probability distribution (commonly Gumbel) fitted to observed maxima (Cook and Mayne, 1980; Ho et al., 2005; St. Pierre et al., 2005). The last method (Gumbel method) is the most flexible among the three, offering a statistical quantification of the peak at a selected fractile rather than a single observed peak or simple average.

The perceived data length requirement of the Gumbel method has led to the development of alternative methods for the estimation of C_{p_peak} from short records. The complete time series is used to estimate a peak CDF from an underlying Gaussian process, and a translation maps this CDF to the peak CDF of the assigned non-Gaussian time series (translation methods). Kareem and Zhao (1994) used the moment-based Hermite polynomial to define the translation between the Gaussian and non-Gaussian processes. Kwon and Kareem (2011) employed an updated and more robust Hermite polynomial model (Winterstein and Kashef, 2000). Sadek and Simiu (2002) modeled the non-Gaussian time

* Corresponding author. Tel.: +1 352 390 9537; fax: +1 352 392 3394.
E-mail addresses: xpeng@ufl.edu (X. Peng), lupingyang@ufl.edu (L. Yang), egavanski@m.tohoku.ac.jp (E. Gavanski), kgurl@ce.ufl.edu (K. Gurley), dprev@ce.ufl.edu (D. Prevatt).

0167-6105/$ - see front matter © 2014 Elsevier Ltd. All rights reserved.
http://dx.doi.org/10.1016/j.jweia.2013.12.013

series by using gamma and Gaussian distributions to fit the long and short tails, respectively. The parameters in the fitted distributions were re-evaluated by using the theoretical moment estimators in Tieleman et al. (2006). Ben Ayed et al. (2011) employed a translation model to full scale pressure data and compared results with values in ASCE 7. Huang et al. (2013) established the mapping relationship between the non-Gaussian CDF and its underlying Gaussian CDF based on a probabilistic model using the kernel smoothing technique.

The minimum wind tunnel testing time interval necessary to estimate C_{p_peak} should be selected within the context of acceptable uncertainty. Sadek et al. (2004) used wind tunnel data to quantify fluctuating internal forces and Monte Carlo simulations of additional time histories to evaluate the sampling error of C_{p_peak} using a translation method. Gavanski et al. (2013) determined the uncertainty of C_{p_peak} estimates produced by the Gumbel method in terms of the time series duration and the number of subsets used to observe the peaks, providing guidance regarding the trade-off between time series duration and C_{p_peak} uncertainty. The current study expands the Gavanski et al. (2013) peak wind pressure estimation uncertainty analysis to include four existing and two new translation methods. This provides a common framework by which to compare the relative strengths and weaknesses of the methods with regard to: (1) time series duration necessary to achieve similar precision and (2) accuracy when applied to mildly and strongly non-Gaussian time series.

It is shown that: (1) the Gumbel method maintains similar accuracy in both mildly and strongly non-Gaussian time series; (2) for mildly non-Gaussian data, the existing translation methods require less data to achieve accuracy comparable to the Gumbel method; (3) for strongly non-Gaussian data, the existing translation methods lose accuracy; and (4) the new translation methods maintain a short data duration requirement, robust accuracy and precision for mildly and strongly non-Gaussian data.

Section 2 provides details of the Gumbel method (observed peak method). Section 3 presents three existing and two new translation methods. Section 4 presents the wind tunnel dataset and comparative performance studies, and Section 5 concludes.

2. Gumbel method

The Gumbel distribution is often used to fit the distribution of peak wind pressure coefficients

$$F_{X_{PK}}(x;t) = \exp\{-\exp[-\alpha_t(x-U_t)]\} \tag{1}$$

where α_t and U_t are the coefficients determined from a series of observed peaks, x is the pressure coefficient, and t is the duration in which a single peak is observed (reference duration). α_t and U_t are determined based upon N observed peaks using one of a number of available methods, as listed in the schematic in Fig. 1. This method requires a total record duration of $t_{total}=Nt$. The resultant cumulative distribution function (CDF) corresponds to the reference duration of t. For example, C_{p_peak} representing a 22% probability of exceedance (POE) within a ten minute reference duration could be estimated by dividing a 160 min record into 16 ten minute segments, observing the largest peak in each segment, estimating the Gumbel parameters using these peaks, and identifying the 22% POE from the Gumbel CDF model.

Cook and Mayne (1980) presented a procedure to convert the Gumbel parameters between different reference durations. This allows the estimation of α_t and U_t using a sufficient N within a relatively short data record, followed by a conversion to the desired longer reference duration T. For the two time reference duration values (t, T, $t<T$), the conversion is (Cook and Mayne, 1980)

$$\alpha_T = \alpha_t \tag{2}$$

$$U_T = U_t + 1/\alpha_t \ln(T/t) \tag{3}$$

C_{p_peak} is then identified as x_{pk} at a chosen fractile in $F_{X_{PK}}$. A subsequent study by Cook (1982) calibrated this method to assess the peak factor and quasi-static approaches to assess wind loads. The accuracy and precision (uncertainty) associated with the Gumbel method with this conversion will be compared with the uncertainties of translations methods in Section 4. Gavanski et al. (2013) showed that the Gumbel method as defined above yields almost identical results to the observed peaks methodology proposed in the ISO (2009) standard.

Kasperski (2003) and Holmes and Cochran (2003) applied the Type III Extreme Value Distribution and three-parameter Generalized Extreme Value Distribution to fit the peak wind pressure coefficients, respectively. Holmes and Cochran (2003) recommended the Gumbel model for its simplicity.

3. Translation methods

A series of studies have presented an alternative methodology for the estimation of the C_{p_peak}. Rather than fitting an extreme value distribution to observed peaks, these methods utilize the entire time series to produce an estimate of C_{p_peak} (Ben Ayed et al., 2011; Kwon and Kareem, 2011; Sadek and Simiu, 2002; Tieleman et al., 2006).

3.1. Translation method concept

Fig. 2 illustrates the translation method to estimate C_{p_peak}. Consider a standardized non-Gaussian record x. This record can be expressed as a translation of a standardized Gaussian process u, and the relation inverted to express u in terms of x

$$x = g(u) \text{ and } u = g^{-1}(x) \tag{4}$$

in which $g(\bullet)$ represents the translation function.

For the underlying Gaussian process u, the CDF of its peak within reference duration t, $F_{U_{PK}}(x;t)$, is (Rice, 1945)

$$F_{U_{PK}}(u;t) = \exp[-\nu_0 t \exp(-u^2/2)] \tag{5}$$

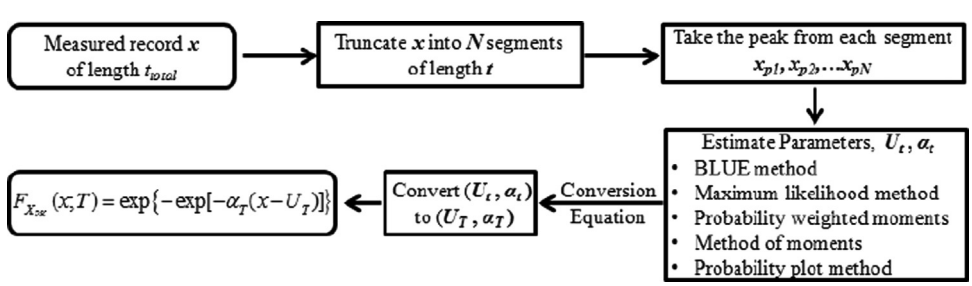

Fig. 1. Observed peak method (Gumbel method).

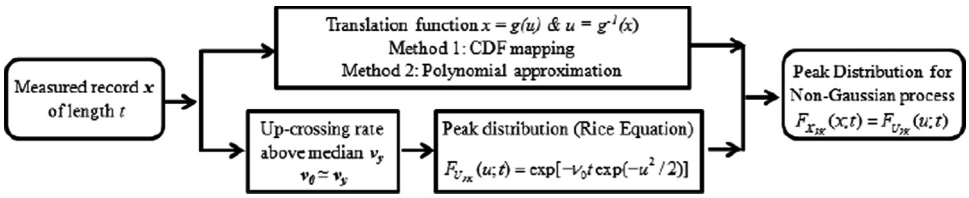

Fig. 2. Translation method.

in which ν_0 is the zero up-crossing rate. ν_0 can be determined by counting the up-crossing rate ν_y of x above its median (y) or computing the spectral ratio (Sadek and Simiu, 2002). The desired CDF of the peak of the non-Gaussian process x within the reference duration t, $F_{X_{PK}}(x;t)$, is obtained by substituting the inverse translation function, Eq. (4), into Eq. (5)

$$F_{X_{PK}}(x;t) = F_{U_{PK}}(u;t) = F_{U_{PK}}[g^{-1}(x);t] = \exp\{-\nu_0 t \exp[-(g^{-1}(x))^2/2]\} \tag{6}$$

C_{p_peak} is then identified as x_{pk} at a chosen fractile in $F_{X_{PK}}$. Various methods have been proposed to determine the translation function $g(\bullet)$. In this study, several translation models are considered: Sadek and Simiu (2002) (CDF mapping), Tieleman et al. (2006) (CDF mapping), Kwon and Kareem (2011) (polynomial approximation), Huang et al. (2013) (CDF mapping) and two new alternatives proposed herein (one polynomial approximation and one CDF mapping). Each is discussed in the following sections.

3.2. Translation method: Sadek and Simiu (2002) – SAD

Sadek and Simiu (2002) identified the parent distribution of the time series by using the probability plot correlation coefficient method (PPCC). The three-parameter gamma distribution and normal distribution were used to fit the long and short tails of the parent distribution, respectively. The translation function is acquired via CDF mapping (Grigoriu, 1995)

$$F_X(x) = \Phi(u) \tag{7}$$

where $F_X(\bullet)$ is the CDF of three parameter gamma distribution, and $\Phi(\bullet)$ is the CDF of the underlying standard normal distribution. This equation establishes a monotonic transformation between x and u.

3.3. Translation method: Tieleman et al. (2006) – TIE

Following Sadek and Simiu (2002), Tieleman et al. (2006) used the method of moments to model the gamma distribution.

3.4. Translation method: Huang et al. (2013) – HUA

Huang et al. (2013) applied the non-parametric kernel smoothing method to determine the probabilistic model of the parent distribution. For the parametric approach the desired distribution is assumed as a particular form, with parameters to be estimated. The non-parametric approach attempts to estimate the probability density directly from the data without assuming a particular distribution form. Kernel density estimation (KDE) is a non-parametric way to estimate the probability density function of a random variable.

Let (x_1, x_2, …, x_M) be a group of samples from an independent and identically distributed random variable with an unknown density function $f_X(x)$. The kernel density estimator is (Li and Scott, 2011)

$$\hat{f}_X(x) = \frac{1}{Mh}\sum_{i=1}^{M} K\left(\frac{x-x_i}{h}\right) \tag{8}$$

where $K(\cdot)$ is the kernel function, which is symmetric but not necessarily positive function. M is the number of sample points. Kernel functions might have many possible choices. However, Gaussian kernel function is commonly used due to its computational advantage, defined as

$$K(x) = \frac{1}{\sqrt{2\pi}}\exp\left(-\frac{x^2}{2}\right) \tag{9}$$

h is a smoothing parameter called the bandwidth, which is obtained as follows (Li and Scott, 2011):

$$h = \left(\frac{4\hat{\sigma}^5}{3M}\right)^{1/5} \tag{10}$$

in which $\hat{\sigma}$ represents the estimate of standard deviation of sample. The kernel method yields smooth estimates in bulk, but behaves badly at the end points.

3.5. Translation method: Kwon and Kareem (2011) – KWO

Hermite polynomials have been demonstrated to be very useful in modeling non-Gaussian data. Winterstein and Kashef (2000) presented a third order Hermite model for a softening translation process

$$x = g(u) \approx k[u + c_3(u^2-1) + c_4(u^3-3u)], \quad k = 1/\sqrt{1+2c_3{}^2+6c_4{}^2} \tag{11}$$

$$c_3 = \frac{\gamma_3}{6}\left[\frac{1-0.015|\gamma_3|+0.3\gamma_3{}^2}{1+0.2\gamma_4}\right], \quad c_4 = c_{40}\left[1-\frac{1.43\gamma_3{}^2}{\gamma_4}\right]^{1-0.1\cdot(\gamma_4+3)^{0.8}},$$

$$c_{40} = \frac{[1+1.25\gamma_4]^{1/3}-1}{10} \tag{12}$$

where c_3 and c_4 are the Hermite polynomial coefficients defined in terms of sample skewness and kurtosis (γ_3, γ_4) via the relationships in Eq. (12). Kwon and Kareem (2011) adopted this model to estimate peak factors using the translation framework. It was observed that the approximate relationship in Eq. (12) loses accuracy as x deviates strongly from Gaussian. This includes values of γ_3 and γ_4 commonly observed from wind loads on low-rise buildings (Yang et al., 2013). Accordingly, the accuracy and precision of estimates of the peak distribution obtained using this model vary with the higher order features of the analyzed dataset.

3.6. Translation method: new method 1: Hermite polynomial model – HPM

Based on accuracy limitations for Eq. (12) observed during the analysis of wind tunnel pressure data on a low rise building, an alternative approximate expression relating the skewness and kurtosis of the measured data and the Hermite polynomial

parameters was developed (Yang et al., 2013):

$$c_3 = 0.1967\gamma_3 - 0.01646\gamma_3\gamma_4 + 0.01809\gamma_3{}^3 + 7.438\times10^{-4}\gamma_3\gamma_4{}^2 - 9.209\times10^{-4}\gamma_3{}^3\gamma_4 - 1.366\times10^{-5}\gamma_3\gamma_4{}^3 + 1.527\times10^{-4}\gamma_3{}^5 + 1.07\times10^{-5}\gamma_3{}^3\gamma_4{}^2 + 8.823\times10^{-8}\gamma_3\gamma_4{}^4 \quad (13)$$

$$c_4 = -0.0721 + 0.03176\gamma_4 - 0.02942\gamma_3{}^2 - 0.00179\cdot\gamma_4{}^2 + 0.002348\gamma_3{}^2\gamma_4 + 5.965\times10^{-5}\gamma_4{}^3 - 6.282\times10^{-4}\gamma_3{}^4 - 6.355\times10^{-5}\gamma_3{}^2\gamma_4{}^2 - 9.692\times10^{-7}\gamma_4{}^4 + 1.497\times10^{-5}\gamma_3{}^4\gamma_4 + 5.457\times10^{-7}\gamma_3{}^2\gamma_4{}^3 + 6.049\times10^{-9}\gamma_4{}^5 \quad (14)$$

Eqs. (11), (13) and (14) establish a translation function which is accurate over a large range of skewness and kurtosis.

In order to guarantee that $g(\bullet)$ and $g^{-1}(\bullet)$ exist (Eq. (4)), the translation function must be monotonic, which requires the following inequality be satisfied:

$$c_3{}^2 + 3c_4(3c_4 - 1) \le 0 \quad (15)$$

Winterstein and MacKenzie (2011) presented an approximation of the monotonic region

$$3 - \gamma_4 + (1.25\gamma_3)^2 \le 0 \quad (16)$$

This defines the range over which the application of the Hermite polynomial model (HPM) is appropriate (Fig. 3). Yang et al. (2013) showed that the wind tunnel pressure data on a low rise building typically fall within this range. For the case of mild deviations from the monotonic region, the HPM is still applicable by adjusting the measured skewness and/or kurtosis such that the resultant combination falls on the border established by Eq. (16). Fig. 3 presents three ways to adjust the skewness and kurtosis: (1) vertical mapping: retain the measured kurtosis and solve for skewness using Eq. (16); (2) Normal mapping: identify the border skewness and kurtosis combination closest to the measured pair; (3) lateral mapping: retain the measured skewness and solve for kurtosis using Eq. (16). The vertical mapping is recommended based on trial and error analysis of the datasets to be described in Section 4.1.

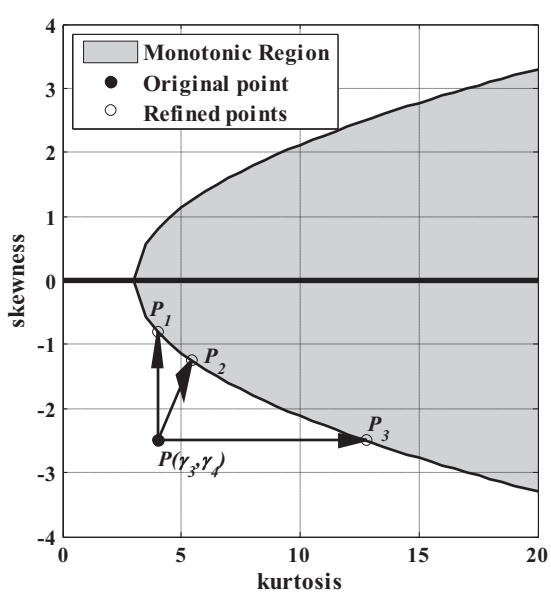

Fig. 3. Monotonic region for the Hermite polynomial translation function as a function of skewness and kurtosis & illustration of vertical, normal and lateral mappings.

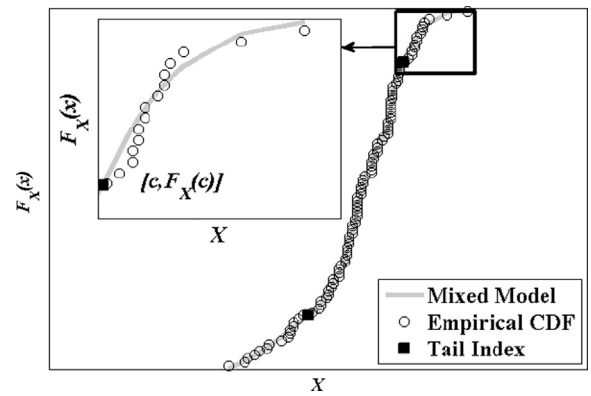

Fig. 4. Mixed probability model of $F_X(x)$.

In this study the HPM [Eqs. (11), (13) and (14)] is utilized as the translation function $g(\bullet)$ in Eq. (4) to estimate C_{p_peak} using the translation framework.

3.7. Translation method: new method 2: mixed distribution model – PAR

A mixed distribution model was investigated to capture both the tail and bulk probability regions. As illustrated in Fig. 4, an empirical distribution from the measured data is applied in the bulk probability region, and a Generalized Pareto distribution (GDP) is applied in the tails. The expression for GPD is (Ramu et al., 2010)

$$F_{par}(x) = P(X \le x | X \ge c) = \frac{P(c \le X \le x)}{P(X \ge c)} = \frac{F_X(x) - F_X(c)}{1 - F_X(c)} = \begin{cases} 1 - [1 - (a(x-c)/b)]^{1/a} & a \ne 0 \\ 1 - \exp[-((x-c)/b)] & a = 0 \end{cases} \quad (17)$$

where c is a location parameter, referred to as the tail-index or threshold of the tails. a and b are the shape and scale parameters, respectively, determined using either maximum likelihood or method of moments applied to the data beyond the selected tail-index c. Only the case of $a \ne 0$ is considered herein. The objective CDF for the tails can be gained via converting Eq. (17)

$$F_X(x) = F_{par}(x)[1 - F_X(c)] + F_X(c), \quad x \ge c \quad (18)$$

where $F_X(c)$ denotes the probability that the data are less than the threshold c, which can be determined using the empirical distribution. The CDF of the mixed probabilistic model is equal to $F_X(c)$ when $x = c$, ensuring that CDF is continuous in value at the tail index point $x = c$. Once the statistical model is determined, the desired translation function is established via CDF mapping, i.e. Eq. (7).

The accuracy of this procedure is sensitive to the selection of the tail-index value c (Ramu et al., 2010). Boos (1984) suggested that for approximately exponential tails, the ratio of k_{Tail} (number of points in tails) over k (total data points) should be 0.2 when $50 \le k \le 500$ and 0.1 when $500 < k \le 50{,}000$. Hasofer (1996) recommended $k_{Tail} = 1.5\sqrt{k}$. In this study the Hasofer (1996) criterion is used to determine the tail-index.

4. Comparative performance study

4.1. Dataset

The surface pressure data used for the comparative performance study are from tests conducted in the Boundary Layer Wind Tunnel II at the University of Western Ontario (UWO). Information about the wind tunnel and data acquisition system can be found in Ho et al. (2005) and Kopp et al. (2010). The wind tunnel tests were

conducted on two 1:50 scale single-story residential houses in suburban exposure (z_0=0.23 m). The full-scale companion structures (FL27 and FL30) are located in the Panhandle of Florida, and collected time histories of pressure data during Hurricane Ivan in 2004 (Ben Ayed et al., 2011; Liu et al., 2009). Only the wind tunnel data are used in the current study. The surface pressure acting at each tap on the model roofs was measured at the reference wind speed of V_{ref}=14.5 m/s and re-referenced to mean roof height (4.3 m) with a sampling rate of 400 Hz. In the case of 120°, 125° and 130° wind approach directions, the test duration is three hours. Assuming a full scale wind speed at 10 m height in suburban terrain (z_0=0.23 m) of 32 m/s (velocity scale=1:5), the sampled data for these three directions are equivalent to 30 h in full scale (time scale=1:10). Figs. 5 and 6 show the test models and tap locations, respectively.

Table 1 summarizes the parameters for the experiment. "Generic" terrain is the case without neighboring houses while the "Detailed" terrain is the case with neighboring houses included. These two models, two terrains and three wind directions yield the 12 test cases used in this study. The skewness and kurtosis obtained from all of taps from these 12 test cases are plotted in Fig. 7, along with the monotonic region for the Hermite model (HPM). All of wind tunnel test data either fall within or are very close to the boundary of the monotonic region, indicating the applicability of HPM. The identified taps in Figs. 6 and 7 provided the records used in the first portion of the comparative performance study (Section 4.3).

The 30 h duration is longer than commonly employed, and provides the means to generate an accurate empirical peak CDF (F_{emp}) and empirical peak pressure coefficient, $C_{p_peak_emp}$, for each tap. This serves as the empirical point of comparison for the Gumbel and translation peak estimation methods applied to a series of short duration (15 min) subsets of the 30 h records in the following analysis.

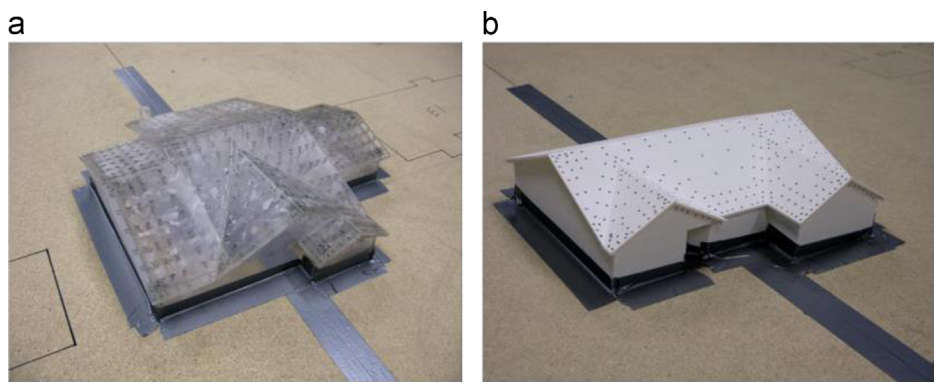

Fig. 5. Two 1:50 scale residential building models. (a) FL27 house model and (b) FL30 house model.

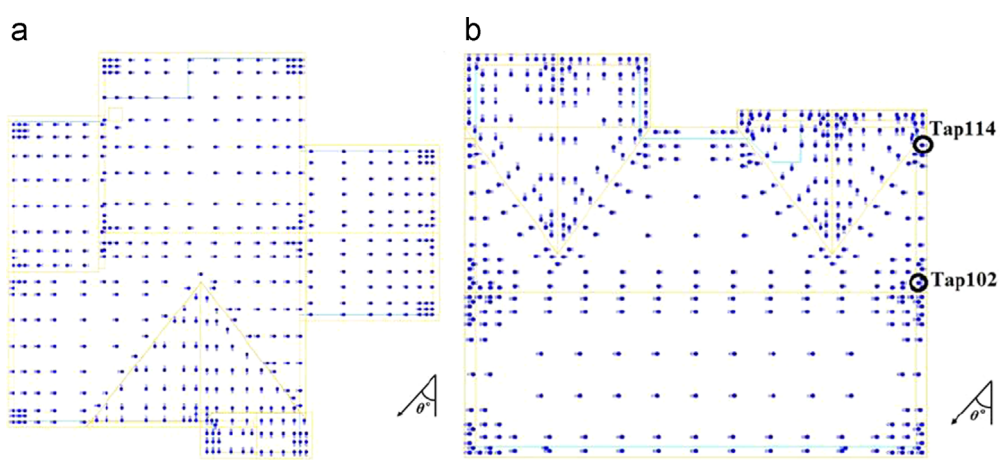

Fig. 6. Layout and test wind direction (θ°) for two 1:50 scale residential building models. (a) FL27 and (b) FL30.

Table 1
Wind tunnel test parameters.

Test models	FL27	FL30
Terrains	Generic, detailed	Generic, detailed
Length scale	1:50	1:50
Time scale	1:10	1:10
Sampling Frequency at model scale (Hz)	400	400
Sampling time in full scale (h)	30	30
Low pass filter cut-off frequency at model scale (Hz)	200	200
Wind direction (deg)	120, 125, 130	120, 125, 130
Wind speed at reference height (m/s)	14.5	14.5
Number of roof taps	496	474

4.2. Comparative performance methodology

The Gumbel and translation methods are now applied to estimate the peak CDF and C_{p_peak} of the wind tunnel data described in the last section. The methodology is first explained and applied to two individual tap records to offer a detailed comparison. The method is then extended to all taps on the 12 test cases (two models, two terrains and three directions).

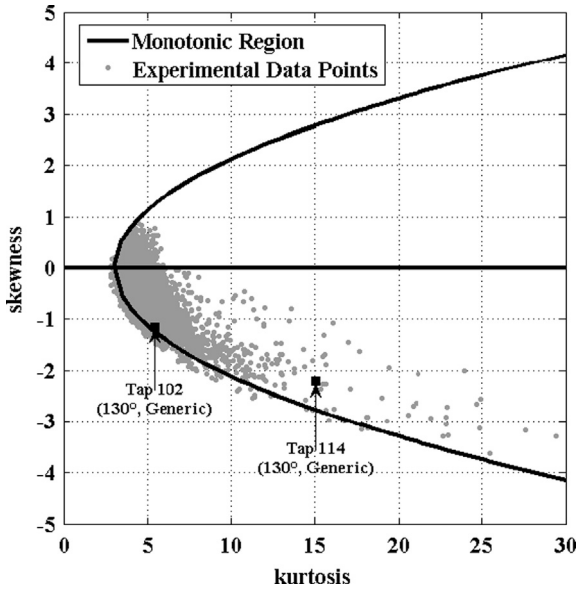

Fig. 7. Skewness and kurtosis from all taps for the 12 test cases, and the monotonic region for HPM.

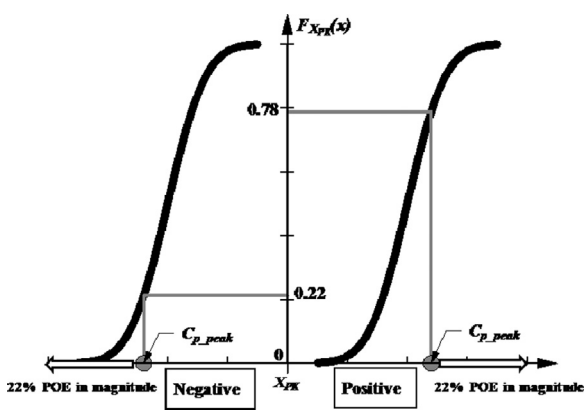

Fig. 8. Definition of 22% probability of exceedance (POE).

The wind tunnel pressure coefficient data at each tap was divided into 120 fifteen minute (full scale) segments. The largest pressure coefficient in magnitude was collected from each segment. These peaks were sorted by magnitude and allocated an empirical CDF value

$$F_{emp} = i/(m+1) \tag{19}$$

where i is the integer vector, 1–120, and $m=120$.

The empirical peak pressure coefficient ($C_{p_peak_emp}$) herein is defined as the 22% fractile of F_{emp} for minima, and the 78% fractile for maxima, as illustrated in Fig. 8. This selection is consistent with Cook and Mayne (1980) and Kasperski (2003). Linear interpolation is applied to the empirical CDF to identify $C_{p_peak_emp}$.

The empirical peak pressure coefficient $C_{p_peak_emp}$ is a random variable with uncertainty that can be expressed as a standard error. The Maritz–Jarrett method to estimate the standard error of a sample median (Maritz and Jarrett, 1978) was extended to the general case of any quantile from an empirical CDF (Wilcox, 2012) and applied herein. The empirical value ($C_{p_peak_emp}$) plus and minus two standard errors represents 95.45% confidence interval, and is utilized in the forthcoming results to represent the uncertainty of the empirical $C_{p_peak_emp}$.

A Monte Carlo study was conducted to verify this standard error quantification. One thousand realizations of measured 30-h records were generated for several taps. A correlation–distortion based non-Gaussian stochastic simulation algorithm was applied to ensure that the power spectral density and probability density function of each realization matched that of the measured record (e.g., Grigoriu, 2009). This produced 1000 simulated empirical CDFs (F_{emp_sim}) and 1000 corresponding simulations of the empirical peak pressure coefficient ($C_{p_peak_emp_sim}$) that represent estimates of $C_{p_peak_emp}$, from which a Monte Carlo based standard error was quantified. For each of the measured 30-h records on which this study was conducted, the resultant Monte Carlo based standard error closely matched that of the extended Maritz–Jarrett standard error (Wilcox, 2012). This verifies the use of the Maritz–Jarrett standard error that is applied in the forthcoming results.

Six translation methods and the Gumbel method were each applied to the 120 fifteen minute segments to generate 120 peak CDFs ($F_{X_{PK}}$) and peak pressure coefficient estimates, $C_{p_peak_est}$, defined as the 22% probability of exceedance from $F_{X_{PK}}$. Each of the seven methods uses a 15 min (full scale) record to produce a single peak pressure coefficient estimate $C_{p_peak_est}$. For each method the

Table 2
Nomenclature.

Definitions	
$C_{p_peak_emp}$	Peak pressure coefficient from empirical cumulative distribution function F_{emp}
$C_{p_peak_est}$	Estimated peak pressure coefficient from modeled cumulative distribution function $F_{X_{PK}}$
F_{emp}	Empirical cumulative distribution function. Reference duration 15 min
$F_{X_{PK}}$	Modeled cumulative distribution function. Reference duration 15 min
MSE	Mean square error between the estimates ($C_{p_peak_est}$) and empirical ($C_{p_peak_emp}$)
PTG	Percentage of estimates ($C_{p_peak_est}$) falling within a range of $C_{p_peak_emp} \pm 2$ standard errors
POE	Probability of exceedance (see Fig. 8)
Peak pressure coefficient estimation methods	
G01	Observed peaks: Gumbel method (reference duration of 1 min, converted to 15 min)
HUA	Translation model proposed by Huang et al. (2013). Reference duration 15 min
HPM	Translation model proposed in this study: Hermite polynomial model. Reference duration 15 min
KWO	Translation model proposed by Kwon and Kareem (2011). Reference duration 15 min
PAR	Translation model proposed in this study: mixed CDF model. Reference duration 15 min
SAD	Translation method proposed by Sadek and Simiu (2002). Reference duration 15 min
TIE	Translation method proposed by Tieleman et al. (2006). Reference duration 15 min

mean of these 120 $C_{p_peak_est}$ determines the accuracy relative to $C_{p_peak_emp}$, and the coefficient of variation among the 120 C_{p_peak} estimates determines the precision of the estimation method. The methods proposed by Sadek and Simiu (2002), Tieleman et al. (2006), Huang et al. (2013), and Kwon and Kareem (2011) are denoted as SAD, TIE, HUA, and KWO, respectively. The two new translation models are denoted as HPM and PAR for the Hermite polynomial model and the Pareto model, respectively. The nomenclature is summarized in Table 2.

The observed peaks Gumbel method was applied to each 15 min segment by extracting $N=15$ peaks from sequential one minute segments, followed by a conversion to the 15 min reference duration using Eqs. (2) and (3), and denoted as G01. The coefficient of variation (COV) among the 15 observed peaks was quantified for every Gumbel $C_{p_peak_est}$, and ranged from 0.064 to 0.285 for the datasets used in this study. This corresponds well with the COV range considered by Kasperski (2003) of 0–0.3.

4.3. Comparative performance: two taps, 130° wind direction, Generic terrain

The time series obtained at two taps (102 and 114, Figs. 6 and 7) are analyzed in this section using the Generic surroundings and the 130° approach direction. Figs. 9 and 10 show the data histogram (HIST) from a single 15 min record from Taps 102 and 114, respectively, and the fitted probability density function from each of the six translation methods used in the comparison. To better observe the model fit in tails, semi-log scales are also provided. The skewness and kurtosis of 30 h time series at Tap 102 (Fig. 6-b) are −1.3035 and 5.7504, respectively. For Tap 114, the skewness and kurtosis are −2.2636 and 15.1778, respectively. Each of the models fit the data well in the left tail in the case of the mildly non-Gaussian record (Tap 102, Fig. 9), while discrepancies can be seen in some of the models for the strongly non-Gaussian record (Tap 114, Fig. 10). The influence of these discrepancies on $C_{p_peak_est}$ will be shown in the next two sections.

4.3.1. Example one: Tap 102 (mildly non-Gaussian data)

Fig. 11 presents the F_{emp} (black dashed line) from the 30 h record and the modeled $F_{X_{PK}}$ obtained from each of the 120 fifteen minute segments (gray lines) for Tap 102. The seven plots delineate the six translation methods and the Gumbel method. Fig. 12 consolidates the results in Fig. 11 by isolating the pressure coefficient corresponding to the 22% POE as defined in Fig. 8. In Fig. 12, the mean of the 120 $C_{p_peak_est}$ is the black boxes. The gray boxes denote the 25th and 75th percentiles from the 120 estimates, and the whiskers represent the 2.5 and 97.5 percentiles. The empirical $C_{p_peak_emp}$ plus and minus two standard errors (Section 4.2) are the dashed and solid black lines, respectively. This range provides a means of comparing the performance of the seven methods.

The mean (black boxes) of all seven methods falls within the two standard error range of the empirical value. This is related to the good match between each of the PDF models and the data histogram as shown in Fig. 9. Five of the methods show similar precision (gray box and whiskers boundaries). The G01 and PAR

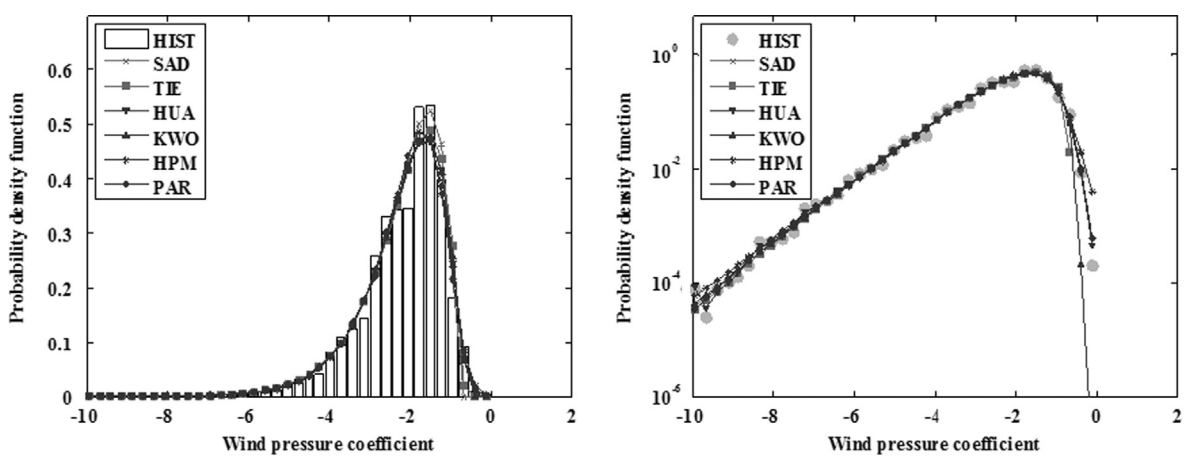

Fig. 9. Comparison of histogram and PDF models fitted to wind tunnel data of Tap 102 on FL30 at a wind angle of 130° (Generic). Left: linear scale and right: semi-log scale.

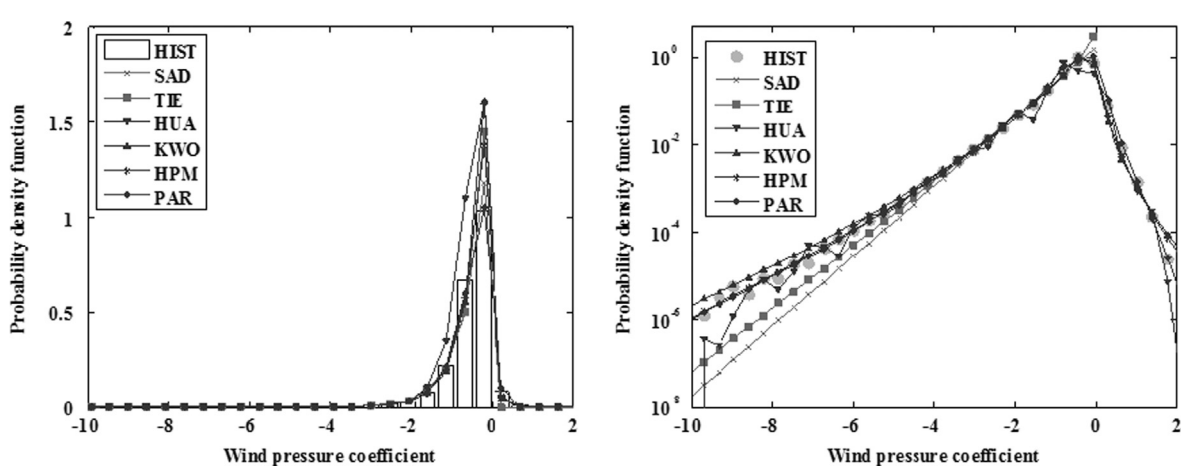

Fig. 10. Comparison of histogram and PDF models fitted to wind tunnel data at Tap 114 on FL30 at a wind angle of 130° (Generic). Left: linear scale and right: semi-log scale.

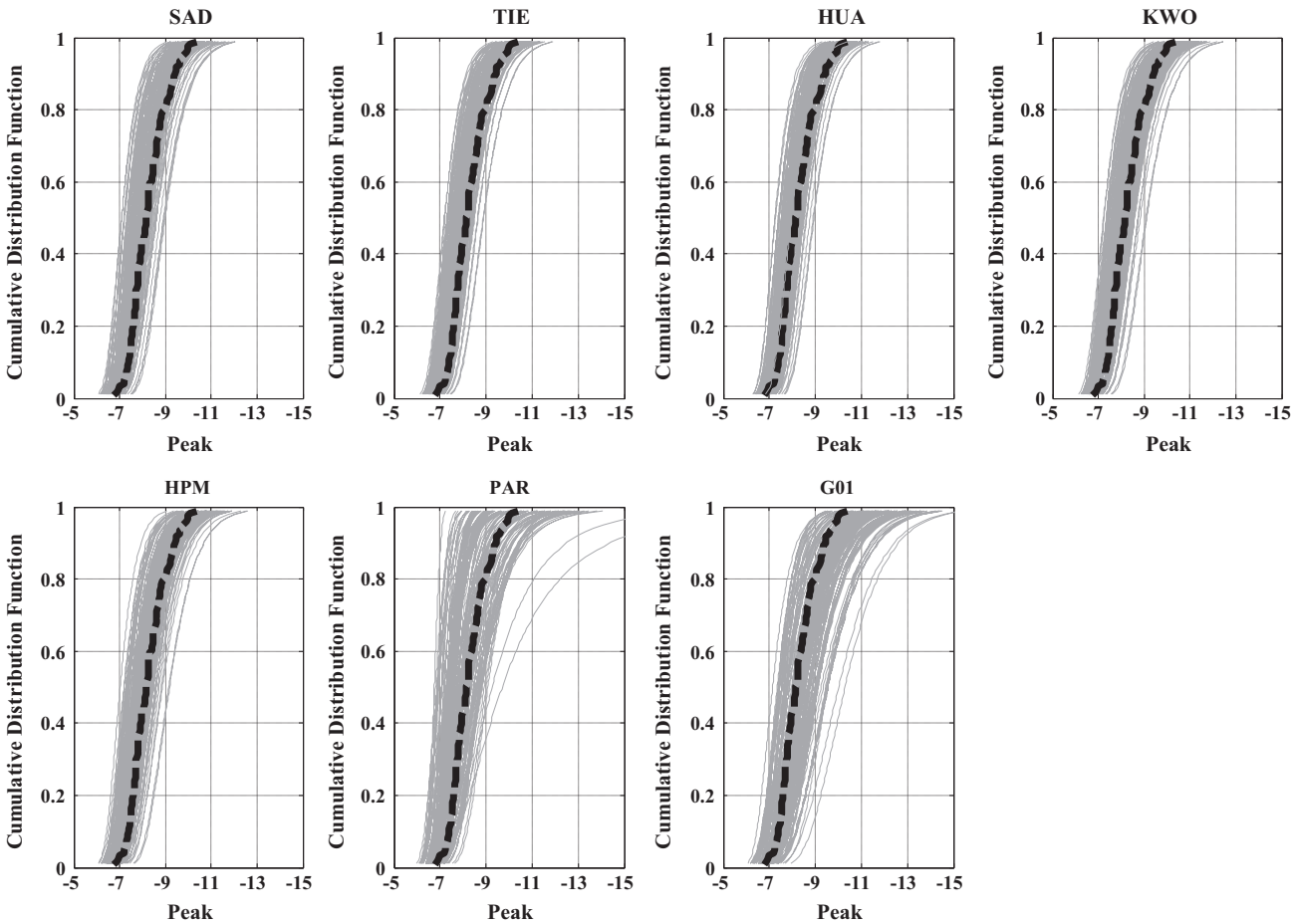

Fig. 11. Empirical CDF, F_{emp} (black dashed line) and estimated CDFs, $F_{X_{PK}}(x, t = 15\text{ min})$ (gray solid lines) for Tap 102.

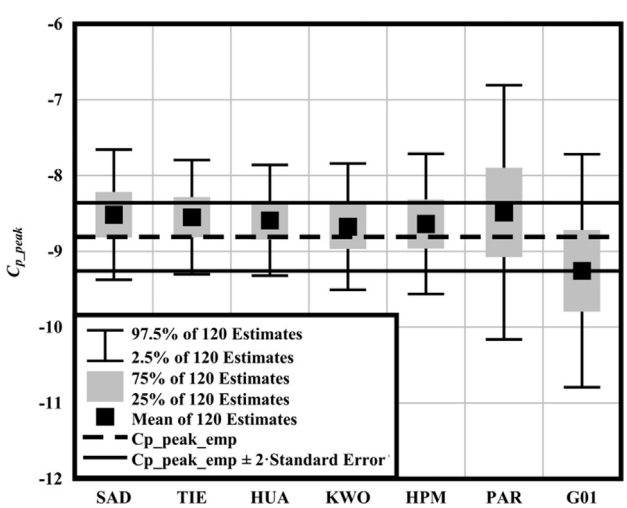

Fig. 12. $C_{p_peak_emp}$ vs. $C_{p_peak_est}$ for Tap 102.

methods display a larger variance among estimates, resulting from samples that fall farther from the 95.45% confidence interval of the empirical estimate. This may be significant if this behavior is consistent for many taps, as in practice only one or a few 15 min samples are used to provide a quantification of expected peaks from a limited length wind tunnel dataset.

KWO and HPM produce very similar results in this example. Both of these methods use the Hermite polynomial translation, and for the case of mildly non-Gaussian data, the coefficient identification equations [Eq. (12) vs. Eqs. (13) and (14)] yield very similar coefficients for the translation in Eq. (11). In the next example it is shown that this similarity of performance is not maintained for data that deviate more significantly from Gaussian. It is also shown that three of the translation methods provide estimates that are not within the empirical range. Following the next example, it will be shown in Section 4.4 that the results of a single example are not sufficient for extrapolating expected performance to other taps in the same or other datasets.

4.3.2. Example two: Tap 114 (strongly non-Gaussian data)

The analysis of the strongly non-Gaussian data from Tap 114 shows a greater disparity of performance among the methods relative to the previous example. Fig. 10 shows that the PDF models from the SAD and TIE translation methods deviate from the histogram in the left tail region, while the HPM and PAR PDF models provide accurate tail representations. This is reflected in the results in Figs. 13 and 14, presented in the same manner as Figs. 11 and 12 described in the previous example.

The $F_{X_{PK}}$ from SAD, TIE, HUA, and KWO each demonstrate a distinct offset from the empirical F_{emp} (Fig. 13). This manifests in Fig. 14 as a loss of accuracy. The statistically inferred 95% bounds of the 120 samples fall entirely outside of the empirical range for SAD, TIE and HUA. In contrast to the previous example, the KWO and HPM results are significantly different, with HPM appearing more accurate and precise. Eq. (12) employed by KWO is not accurate for strongly non-Gaussian data, while Eqs. (13) and (14) used in HPM maintain accuracy (Yang et al., 2013).

Comparing the performance of each method with itself between Figs. 12 and 14 shows that only HPM, PAR and G01

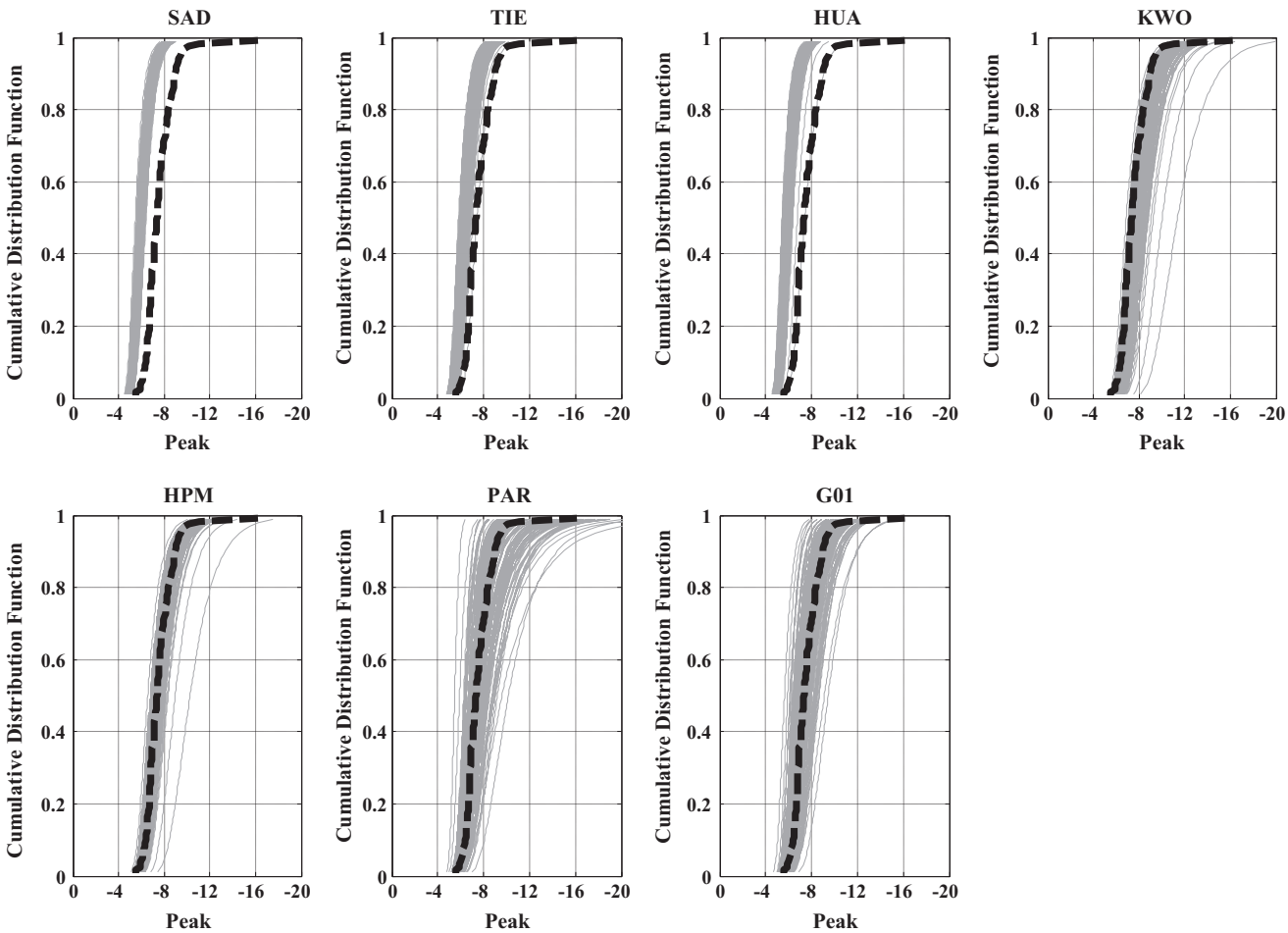

Fig. 13. Empirical CDF, F_{emp} (black dashed line) and estimated CDFs, $F_{X_{PK}}(x, t = 15\text{ min})$ (gray solid lines) for Tap 114.

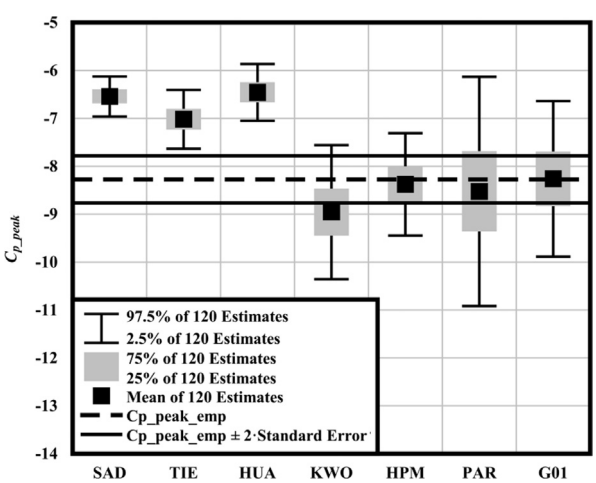

Fig. 14. $C_{p_peak_emp}$ vs. $C_{p_peak_est}$ for Tap 114.

demonstrate stability as the probability content of the data varies from mildly to strongly non-Gaussian. A typical dataset from a wind tunnel experiment usually consist of records with a wide range of probability content (e.g., Fig. 7). In this context it is clear that methods with stabile performance are more desirable than methods that are highly accurate and precise over only a subset of a complete dataset. The next section expands the study to all roof taps in multiple datasets in order to further quantify relative performance.

4.4. Comparative performance: all taps on FL30, 130° wind direction, Generic terrain

The two previous examples are useful to show the potential weaknesses and strengths of the peak pressure coefficient estimation methods under consideration as the probability content of the data varies. The HPM, PAR and G01 methods demonstrated stable performance for both mildly and strongly non-Gaussian data. However, valid conclusions are premature absent a more extensive evaluation. This section applies the performance assessment methodology to all roof taps in Fig. 6-b (130° wind direction, Generic terrain) using scatter plots and a variation of the mean squared error (MSE) as a metric for performance evaluation, defined as

$$MSE = \frac{1}{m}\sum_{j=1}^{m} S_j^2 \tag{20}$$

$$S_j = \begin{cases} C_{p_peak_est}(j) - [C_{p_peak_emp} + 2SE], & C_{p_peak_emp} + 2SE < C_{p_peak_est}(j) \\ 0, & C_{p_peak_emp} - 2SE \le C_{p_peak_est}(j) \le C_{p_peak_emp} + 2SE \\ C_{p_peak_est}(j) - [C_{p_peak_emp} - 2SE], & C_{p_peak_emp} - 2SE > C_{p_peak_est}(j) \end{cases} \tag{21}$$

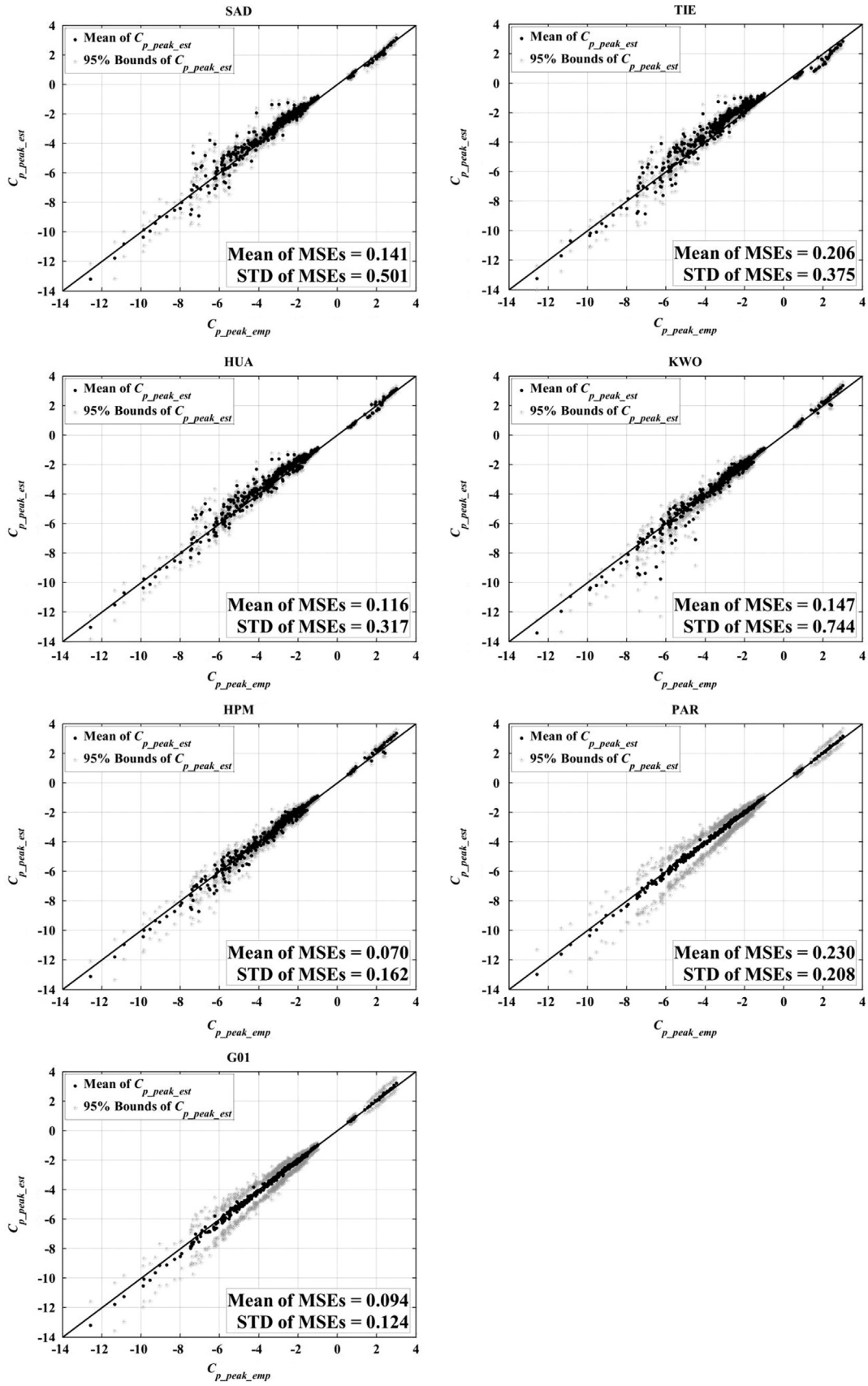

Fig. 15. Comparison of empirical and modeled 22% POE of all roof taps on FL30 at 130° (Generic).

where m represents the number of estimates $C_{p_peak_est}$ from a 30 h record ($m=120$), and SE is the standard error associated with $C_{p_peak_emp}$. In this variation, the error S_j is the difference between the estimate $C_{p_peak_est}$ and the closest border of the empirical range $C_{p_peak_emp}$ +/− two standard errors. $C_{p_peak_est}(j)$ is the jth estimated peak pressure coefficient at each tap. If any given

$C_{p_peak_est}(j)$ is within the empirical range, its contribution to the error summation is zero.

Fig. 15 presents the results from the seven methods using all 474 roof taps on FL30 with $\theta = 130^\circ$, Generic terrain. The abscissa represents the empirical peak pressure coefficient, $C_{p_peak_emp}$, and the ordinate is the estimated pressure coefficients, $C_{p_peak_est}$. The mean (black dot) and 2.5th and 97.5th percentiles (gray stars) from the 120 estimates $C_{p_peak_est}$ for each tap are plotted. The black

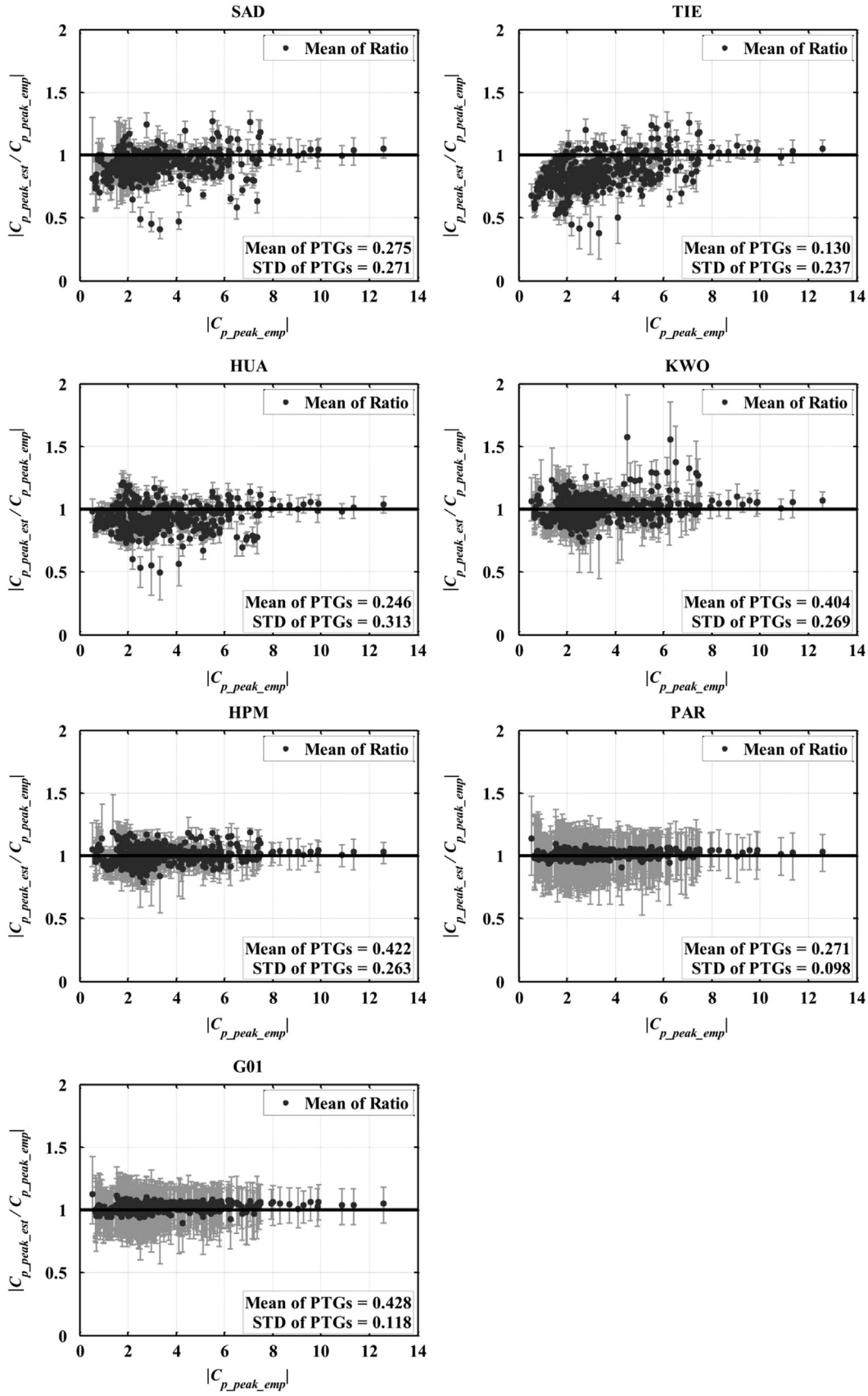

Fig. 16. Ratio of modeled to empirical 22% POE values of all roof taps on FL30 at 130° (Generic).

solid line indicates equality of estimated peaks ($C_{p_peak_est}$) and empirical peaks ($C_{p_peak_emp}$). MSE (Eqs. 20 and 21) was calculated for each individual tap. The average and standard deviation (STD) of the MSE among all taps are provided in the bottom right corner of each plot. The average MSE provides some measure of the accuracy of the method, while the MSE STD provides a measure of the stability of this accuracy from tap to tap.

PAR and G01 appear to be the most consistently accurate with respect to the average of 120 estimates, shown by the close conformity of the black dots with the solid black line. However, given that the intended application of these methods is to a single or a few short records, these mean values (black dots) are never realized. Rather, the outcome in practice is a sample from within the vertical range of the gray stars. Thus, the MSE is a more significant metric for performance evaluation than visual inspection. HPM has the lowest average MSE, accompanied by a low MSE STD. KWO shows more scatter than HPM, and has a much larger MSE STD. SAD, HUA and TIE visually have more scatter than the other methods, quantified by higher average MSE and relatively large MSE STD.

In Fig. 15 it appears that the precision and accuracy of $C_{p_peak_est}$ vary as a function of the magnitude of $C_{p_peak_emp}$. In order to see this more clearly, the results in Fig. 15 are recast in Fig. 16 by normalizing the vertical axis by $C_{p_peak_emp}$. An additional comparative performance metric is introduced for each tap as the fraction of the 120 $C_{p_peak_est}$ that fall within the empirical range $C_{p_peak_emp}$ plus and minus two standard errors (denoted as PTG). The average PTD and standard deviation of the PTG among all taps are provided in the lower right corner of each plot. Each black dot represents the mean value of the 120 ratios at one tap. The gray range about each mean value is the 95% bounds from the 120 ratios. The accuracy and precision of all the seven methods improve with increasing magnitude of the peak pressure coefficient. The overall superior accuracy of PAR and G01 and the precision of HPM are visible. HPM and G01 have the largest PTG scores.

The two new translation methods (PAR and HPM) are clearly more robust than the translation methods in the literature. The Gumbel fitting method (G01) performs well, but demonstrates slightly less precision than HPM at large C_{p_peak} values.

4.5. Comparative performance: 12 test cases from FL27 and FL30

The previous section presented an analysis of all taps from one of the twelve test cases discussed in Section 4.1. In this section, all roof taps from twelve test cases are analyzed (two models, three wind directions and two local terrains), using C_{p_peak} at the 22% POE level. This dataset contains a wide array of mildly and strongly non-Gaussian time histories (Fig. 7). In order to condense the results, only the mean and standard deviation of MSE and PTG metrics are presented.

Fig. 17 presents the average and standard deviation from the MSEs calculated at each tap and each of the twelve test cases. The results in all the cases are consistent with those observed in the previous section. The results of the single test case in the previous section are identified in Figs. 17 and 18 with a box. HPM consistently has the lowest average MSE and among the lowest MSE STD for all cases, indicating an accurate peak value estimate with good stability from tap to tap. The Gumbel method (G01) has the second lowest average MSE in ten of the twelve cases, and among the lowest MSE STD for all cases.

Fig. 18 presents the average and standard deviation from the PTGs calculated at each tap and each of the twelve test cases. Recall that the PTG is the fraction of individual peak estimates

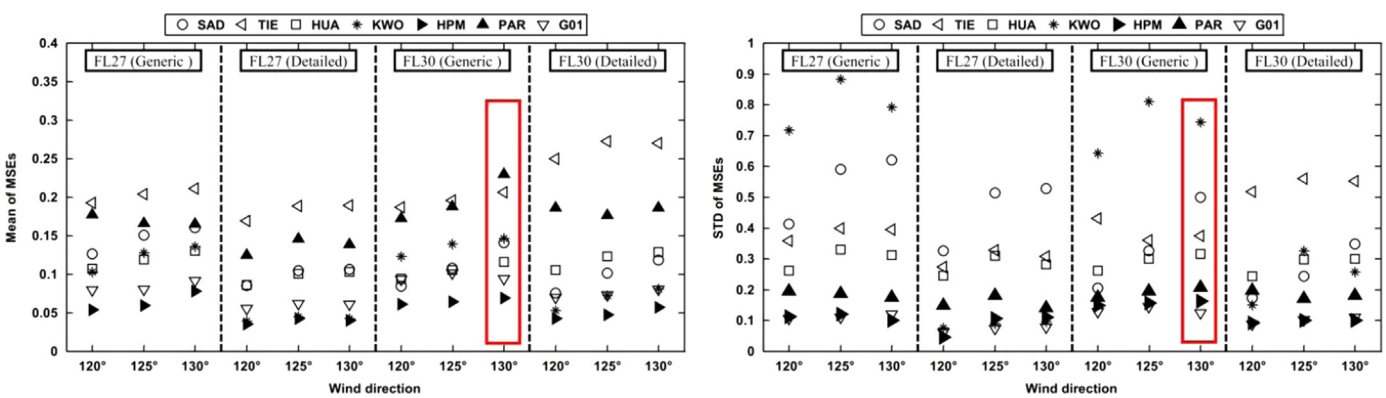

Fig. 17. MSE analysis for 12 test cases at 22% POE level. Left: mean of MSEs and right: STD of MSEs.

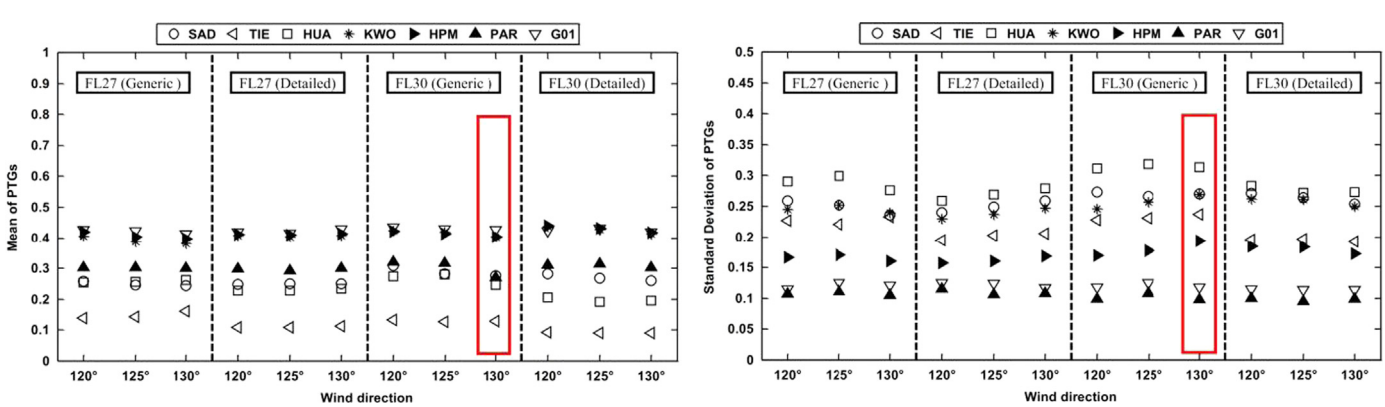

Fig. 18. PTG analysis for 12 test cases at 22% POE level. Left: mean of PTGs and right: STD of PTGs.

($C_{p_peak_est}$) that fall within two standard errors of $C_{p_peak_emp}$. The means of PTGs for the KWO, HPM and G01 methods are very close and consistently higher than the other methods. However, the standard deviation of the PTGs for KWO is consistently higher than that of the HPM and G01, and indicates less stability for KWO relative to HPM and G01.

The results in Figs. 17 and 18 suggest that, among the seven methods considered, HPM and G01 are the most robust and reliable methods for short record peak pressure coefficient estimation. PAR does not appear to offer any significant performance advantage relative to the four existing translation methods. PAR is currently being revisited by the authors to evaluate whether this performance can be improved.

5. Conclusions

In this paper, two procedures are developed for estimating the peak distribution of non-Gaussian wind tunnel pressure coefficients measured on two low rise buildings. One is a modification to the Hermite polynomial probability model (HPM) and is applied within a translation framework. The other is a mixed PDF translation model (PAR), which is developed using the empirical distribution in the bulk and Pareto distributions in tails. Their accuracy and precision relative to empirical distributions obtained from 30 h time histories are evaluated along with four existing translation methods and the Gumbel observed peaks method.

Analysis of one mildly non-Gaussian and one strongly non-Gaussian time series demonstrates that the accuracy and precision of the seven estimation methods under consideration are comparable when the data are mildly non-Gaussian. However, only the HPM and Gumbel (G01) methods offer consistent performance in the case of strongly non-Gaussian data. The performance evaluation methodology is extended to all taps on multiple data sets to provide a quantitative comparison of precision, accuracy and stability of the methods. The HPM and Gumbel (G01) peak methods are shown to be robust with respect to the severity of the non-Gaussian data, and the most accurate and precise among the seven models considered when applied to 15 min segments of twelve wind tunnel data sets measured from two low rise building models. The PAR does not appear to offer a significant improvement over the four existing translation methods considered.

Acknowledgments

This work was supported by NSF CMMI-0928563, the Florida Division of Emergency Management and a University of Florida Alumni Fellowship.

References

Ben Ayed, S., Aponte-Bermudez, L.D., Hajj, M.R., Tieleman, H.W., Gurley, K.R., Reinhold, T.A., 2011. Analysis of hurricane wind loads on low-rise structures. Eng. Struct. 33 (12), 3590–3596.
Boos, D.D., 1984. Using extreme value theory to estimate large percentiles. Technometrics 26 (1), 33–39.
Cook, N.J., 1982. Calibration of the quasi-static and peak-factor approaches to the assessment of wind loads against the method of Cook and Mayne. J. Wind Eng. Ind. Aerodyn. 10 (3), 315–341.
Cook, N.J., Mayne, J.R., 1980. A refined working approach to the assessment of wind loads for equivalent static design. J. Wind Eng. Ind. Aerodyn. 6 (1–2), 125–137.
Davenport, A.G., 1964. Note on the distribution of the largest value of a random function with application to gust loading. Proc. Inst. Civil Eng. 6739, 187–196.
Gavanski, E., Gurley, K.R., Kopp, G.A., 2013. Uncertainties in the estimation of peak pressures on low-rise buildings with Gumbel fitting approach. In: Proceedings of the 12th Americans Conference on Wind Engineering, Seattle, WA.
Gioffrè, M., Gusella, V., Grigoriu, M., 2000. Simulation of non-Gaussian field applied to wind pressure fluctuations. Probab. Eng. Mech. 15 (4), 339–345.
Grigoriu, M., 1995. Applied Non-Gaussian Processes: Examples, Theory, Simulation, Linear Random Vibration, and MATLAB Solutions. PTR Prentice Hall, Englewood Cliffs, NJ.
Grigoriu, M., 2009. Existence and construction of translation models for stationary non-Gaussian processes. Probab. Eng. Mech. 24 (4), 545–551.
Hasofer, A., 1996. Non-Parametric Estimation of Failure Probabilities. Mathematical Models for Structural ReliabilityCRC Press, Boca Raton, Florida, USA, pp. 195–226.
Ho, T.C.E., Surry, D., Morrish, D., Kopp, G.A., 2005. The UWO contribution to the NIST aerodynamic database for wind loads on low buildings: Part 1. Archiving format and basic aerodynamic data. J. Wind Eng. Ind. Aerodyn. 93 (1), 1–30.
Holmes, J.D., Cochran, L.S., 2003. Probability distributions of extreme pressure coefficients. J. Wind Eng. Ind. Aerodyn. 91 (7), 893–901.
Holmes, J.D., Melbourne, W.H., Walker, G.R., 1989. A Commentary on the Australian Standard for Wind Loads AS 1170 Part 2. Australian Wind Engineering Society, Melbourne.
Huang, M., Lou, W., Chan, C., Lin, N., Pan, X., 2013. Peak distributions and peak factors of wind-induced pressure processes on tall buildings. J. Eng. Mech. 139 (12), 1744–1756.
ISO, 2009. ISO 4354: 2009 Wind actions on structures. International Standard Organization.
Kareem, A., Zhao, J., 1994. Analysis of non-gaussian surge response of tension leg platforms under wind loads. J. Offshore Mech. Arct. Eng. 116, 137–144.
Kasperski, M., 2003. Specification of the design wind load based on wind tunnel experiments. J. Wind Eng. Ind. Aerodyn. 91 (4), 527–541.
Kopp, G., Morrison, M., Gavanski, E., Henderson, D., Hong, H., 2010. "Three Little Pigs" project: hurricane risk mitigation by integrated wind tunnel and full-scale laboratory tests. Nat. Hazards Rev. 11 (4), 151–161.
Kwon, D.K., Kareem, A., 2011. Peak factors for non-gaussian load effects revisited. J. Structural Eng. 137 (12), 1611–1619.
Li, Q., Scott, R.J., 2011. Nonparametric Econometrics Theory and Practice. Princeton University Press, Princeton.
Lieblein, J., 1974. Efficient Methods of Extreme-Value Methodology. National Bureau of Standards, Washington, D.C.
Liu, Z., Prevatt, D.O., Aponte-Bermudez, L.D., Gurley, K.R., Reinhold, T.A., Akins, R.E., 2009. Field measurement and wind tunnel simulation of hurricane wind loads on a single family dwelling. Eng. Struct. 31 (10), 2265–2274.
Maritz, J.S., Jarrett, R.G., 1978. A note on estimating the variance of the sample median. J. Am. Stat. Assoc. 73 (361), 194–196.
Peterka, J.A., 1983. Selection of local peak pressure coefficients for wind tunnel studies of buildings. J. Wind Eng. Ind. Aerodyn. 13 (1–3), 477–488.
Ramu, P., Kim, N.H., Haftka, R.T., 2010. Multiple tail median approach for high reliability estimation. Struct. Saf. 32 (2), 124–137.
Rice, S.O., 1945. Mathematical analysis of random noise. Bell Syst. Tech. J. 24 (1), 46–156.
Sadek, F., Diniz, S., Kasperski, M., Gioffre, M., Simiu, E., 2004. Sampling errors in the estimation of peak wind-induced internal forces in low-rise structures. J. Eng. Mech. 130 (2), 235–239.
Sadek, F., Simiu, E., 2002. Peak non-Gaussian wind effects for database-assisted low-rise building design. J. Eng. Mech. 128, 530–539 (Compendex).
St. Pierre, L.M., Kopp, G.A., Surry, D., Ho, T.C.E., 2005. The UWO contribution to the NIST aerodynamic database for wind loads on low buildings: Part 2. Comparison of data with wind load provisions. J. Wind Eng. Ind. Aerodyn. 93 (1), 31–59.
Stathopoulos, T., 1979. Turbulent Wind Action on Low Rise Buildings (Ph.D.). University of Western Ontario, London, Ontario, Canada.
Stathopoulos, T., 1983. Fluctuating wind pressures on low building roofs. J. Struct. Eng. ASCE 109 (1), 266–271, (Proc. Paper 17602–6).
Tieleman, H.W., Elsayed, M.A.K., Hajj, M.R., 2006. Peak wind load comparison: theoretical estimates and ASCE 7. J. Struct. Eng. 132 (7), 1150–1157.
Wilcox, R.R., 2012. Introduction to Robust Estimation and Hypothesis Testing. Academic Press, Amsterdam; Boston.
Winterstein, S.R., Kashef, T., 2000. Moment-based load and response models with wind engineering applications. J. Sol. Energy Eng., Trans. ASME 122 (3), 122–128.
Winterstein, S.R., MacKenzie, C.A., Extremes of nonlinear vibration: models based on moments, l-moments, and maximum entropy. In: Proceedings of the ASME 2011 30th International Conference on Ocean, Offshore and Arctic Engineering, OMAE2011, June 19, 2011–June 24, 2011, American Society of Mechanical Engineers. pp. 617–626.
Yang, L., Gurley, K.R., Prevatt, D.O., 2013. Probabilistic modeling of wind pressure on low-rise buildings. J. Wind Eng. Ind. Aerodyn. 114 (0), 18–26.